JACS
JOURNAL OF THE AMERICAN CHEMICAL SOCIETY

ARTICLE

pubs.acs.org/JACS

Measurement and Statistical Analysis of Single-Molecule Current−Voltage Characteristics, Transition Voltage Spectroscopy, and Tunneling Barrier Height

Shaoyin Guo,[†] Joshua Hihath,[†] Ismael Díez-Pérez,[†,‡] and Nongjian Tao*[,†]

[†]Center for Bioelectronics and Biosensors, Biodesign Institute, and Departments of Electrical Engineering, Arizona State University, Tempe, Arizona 85287, United States

[‡]Department of Physical Chemistry, University of Barcelona, Barcelona 08028, Spain

Supporting Information

ABSTRACT: We report on the measurement and statistical study of thousands of current−voltage characteristics and transition voltage spectra (TVS) of single-molecule junctions with different contact geometries that are rapidly acquired using a new break junction method at room temperature. This capability allows one to obtain current−voltage, conductance voltage, and transition voltage histograms, thus adding a new dimension to the previous conductance histogram analysis at a fixed low-bias voltage for single molecules. This method confirms the low-bias conductance values of alkanedithiols and biphenyldithiol reported in literature. However, at high biases the current shows large nonlinearity and asymmetry, and TVS allows for the determination of a critically important parameter, the tunneling barrier height or energy level alignment between the molecule and the electrodes of single-molecule junctions. The energy level alignment is found to depend on the molecule and also on the contact geometry, revealing the role of contact geometry in both the contact resistance and energy level alignment of a molecular junction. Detailed statistical analysis further reveals that, despite the dependence of the energy level alignment on contact geometry, the variation in single-molecule conductance is primarily due to contact resistance rather than variations in the energy level alignment.

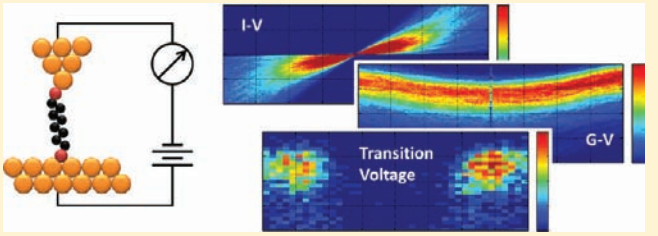

INTRODUCTION

Measuring electron transport in a single molecule bridged between two electrodes is a basic task in understanding the electronic properties of single molecules and designing molecular junctions with desired device functions.[1−4] Due to the large variability in the molecule−electrode contact geometry and the sensitive dependence of the electron transport properties on the atomic-scale details of the contact, the repeated formation and measurement of single-molecule junctions and statistical analyses of these individual junctions have been introduced and used to characterize the conductance of a single molecule. The mechanically controllable break junction (MCBJ),[5−7] and the scanning tunneling microscope (STM) break junction methods[8−10] have been widely employed to make these measurements. The statistical analysis of a large number of molecular junctions with different contact geometries reveals peaks in the conductance histograms, which are used to determine the most probable conductance of a single-molecule junction.[8] This approach allows for meaningful comparisons between experimental data obtained by different groups and between experiments and theories.[11−15]

Despite the success, the combined break junction measurement and conductance histogram approach at room temperature is primarily limited to determining the conductance at a fixed bias. This is because the lifetime of a single molecule bridged across two electrodes is relatively short[16−23] in a typical STM break junction experiment, making it difficult to perform more detailed measurements, such as current−voltage ($I-V$), and conductance-voltage ($G-V$) characteristics. Compared to a fixed low-bias conductance, $I-V$ curvescontain significantly more information, and are a basic requirement for device characterization. A capability to rapidly measure the $I-V$ characteristics of a large number of single-molecule junctions is thus of great importance for developing a better understanding of the charge transport mechanisms in single-molecule junctions, and characterizing the junctions' device functions.

In the present work, we report on an approach to rapidly acquire thousands of $I-V$ and $G-V$ curves of single-molecule junctions at room temperature and carry out a statistical analysis of these curves, thus adding a new dimension (voltage) to the conductance histogram analysis. More importantly, this method allows us to obtain transition voltage spectra (TVS) of the individual molecular junctions.[24−31] Statistical analysis of the TVS of many single-molecule junctions provides detailed information about the tunneling barrier height, or more precisely,

Received: August 19, 2011
Published: October 12, 2011

the alignment between molecular orbital level and the electrode Fermi level, as well as the dependence of the energy level alignment on the detailed contact geometry.We have studied n-alkanedithiols (n = 6, 8 and 10) consisting of linear saturated C−C bonds, and biphenyldithiol, containing conjugate aromatic structures.

EXPERIMENTAL SECTION

We started each measurement by bringing an STM tip into contact with a gold substrate with a small bias voltage applied between the tip and substrate. The tip was then pulled away from the substrate, during which the current between the tip and substrate was monitored. Such a current vs pulling distance curve is referred to as a current or conductance trace. As we have reported previously,[8] steps appear in the current traces when sample molecules bridge between the tip and substrate electrodes via linker groups, such as thiols. The lowest current steps are assigned to single-molecule junctions, which is supported by simultaneously obtained conductance and breakdown force measurement.[18,32] In a typical STM break junction experiment, a large number of conductance traces are recorded and analyzed in the form of conductance histograms from which the single-molecule conductance is determined. In contrast, in the present work, once a step was detected, the tip was held still while the bias voltage was automatically swept for one cycle to produce an $I-V$ curve.After the voltage sweep, the tip was pulled further away from the substrate by a given distance while the current level was checked to determine if the molecular junction was still intact. If so, another $I-V$ curve was recorded, and the process continued until the step collapsed as the molecular junction broke, which was indicated by the sudden drop of current. At that point, the whole procedure started over, and this process was repeated thousands of times. We provide further experimental details in the Supporting Information (SI).

Figure 1a shows a typical current trace in logarithmic scale with stepwise features for octanedithiol (C8), where the coloredspots along the step mark the positions where the individual $I-V$ curves were measured. Figure 1b shows the $I-V$ characteristics obtained at those positions in corresponding colors. The process was then repeated thousands of times, such that a large number (>2000) of $I-V$ curves from different molecular junctions with varying contact geometries were obtained.

RESULTS AND DISCUSSION

***I−V* Histogram.** Figure 2a plots over 2000 such $I-V$ curves for C8, where the color scale represents the occurrence or count number of a current value. The count numbers in the high bias regimes are lower than those in the low-bias regimes, which is due to the divergence of the $I-V$ curves at high bias voltages, rather than incomplete $I-V$ curves. We did encounter incomplete $I-V$ curves because of the breakdown of the molecular junctions at high bias voltages (e.g., Figure S1 in the SI).[33−35] These incomplete $I-V$ curves were not included in the $I-V$ histogram shown in Figure 2a. We also occasionally encounter large telegraphic switching in the $I-V$ curves,[7] which were also excluded from the statistical analysis. These incomplete and switching $I-V$ curves constituted∼30% of all the curves for a bias range of ±0.5 V, which were *automatically* detected using the algorithm described in the SI. The percentage of incomplete $I-V$ curves increased with the bias sweep range due to the instability of the single-molecule junctions at high bias voltages.[34] For example, for a bias range of ±2 V (e.g., Figure 2a) the percentage of incomplete $I-V$ curves increased to 50−70% for C8. The breakdown voltage varies from molecule to molecule, and also junction to junction, and has been attributed to current-induced heating in literature.[33−36]

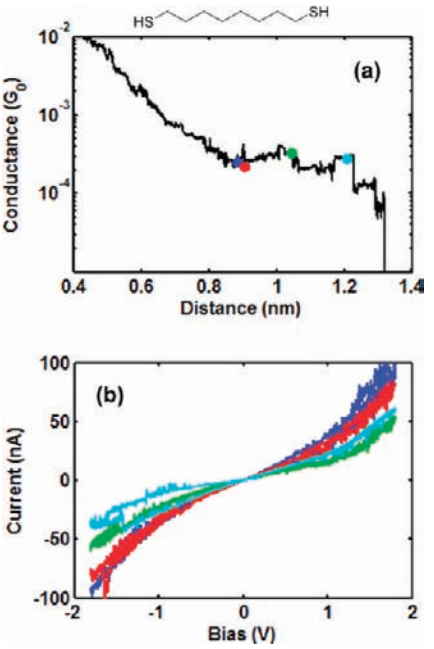

Figure 1. Typical current traces and $I-V$ curves for octanedithiol (C8). (a) Current trace in logarithmic scale showing stepwise features, where colored spots along the step mark the positions where the individual $I-V$ curves were measured. (b) The corresponding $I-V$ curves, in which the colors of $I-V$ curves match the color of spots.

***G−V* Histogram.** From the individual $I-V$ curves, we constructed $G-V$ curves, where $G = I/V$ is the conductance. Note that this conductance should be distinguished from differential conductance, which is defined as $g = dI/dV$. These $G-V$ curves are plotted together in logarithmic scale to form a two-dimensional (2-D) conductance histogram (Figure 2b), where the color scale represents counts at a fixed conductance value and bias voltage. The 2-D conductance histogram shows a clear bowl-shaped red band, corresponding to the distribution of $G-V$ curves within a certain conductance range, from which most the probable $G-V$ curve can be determined. The bowl-shape is present because the current increase is nonlinear with bias in the $I-V$ characteristics, as is discussed in detail below. Such a 2-D conductance histogram contains richer information than the 1-D conductance histogram analysis used in the previous STM break junction experiments. For example, we can directly obtain the "standard" 1-D conductance histogram at various different bias voltages by simply taking vertical profiles from the 2-D histograms. Figure 2c shows several 1-D conductance histograms where each pronounced peak indicates the most probable conductance value at the corresponding bias. The peak shifts toward higher conductance values with bias voltage due to the nonlinearity of the $I-V$ curves.

Previous works observed multiple conductance peaks at low-bias voltages in the alkanedithiols.[12,13,17,37−41] This is clearly confirmed in the $I-V$ curve histogram and the 2-D conductance histogram. Figure 2d shows an $I-V$ curve histogram of C8 recorded with a higher gain setting in the current amplifier than that used to record the $I-V$ curves shown in Figure 2a. This gain setting allowed us to measure lower conductance values of the C8 junctions. The distribution of the $I-V$ curves falls into two distinct bands, which are marked with two dashed lines. The corresponding 2-D conductance histogram ($G-V$ histogram)

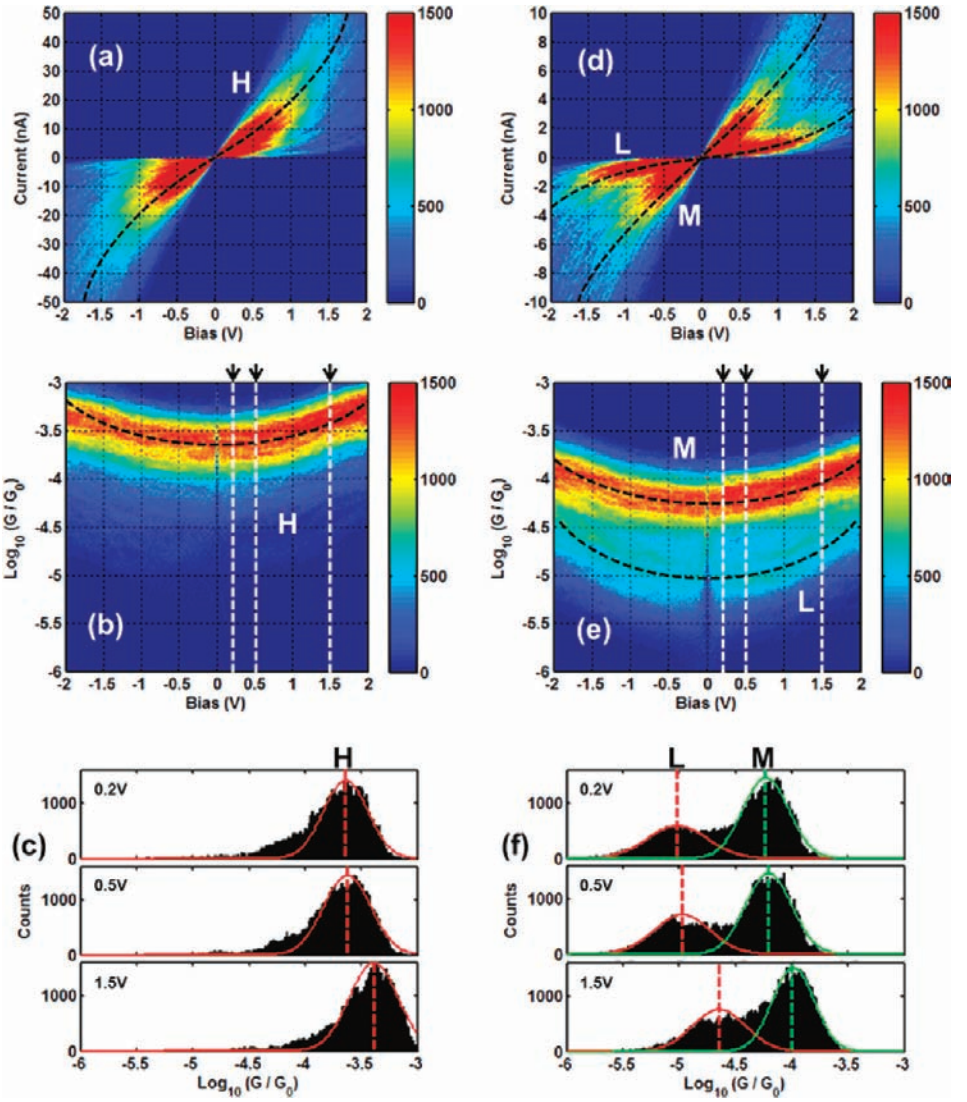

Figure 2. $I-V$ and $G-V$ histograms for C8. (a) $I-V$ histogram for H-junctions consisting of 2151 curves. (b) $G-V$ histogram for H-junctions. (c) 1-D conductance histogram at different bias voltages for H-junctions. (d) $I-V$ histogram for M- and L-junctionsconsisting of 1661 curves. (e) $G-V$ histogram for M- and L-junctions. (f) 1-D conductance histogram at different bias voltages for M- and L-junctions.

is shown in Figure 2e, and the 1-D conductance histograms at several bias voltages are presented in Figure 2f, showing two peaks more clearly. We denote the molecular junctions in Figure 2a,b as H-junctions, and the two distinct sets of junctions in Figure 2d,e as M- and L-junctions, based on their conductance values (H- for high, M- for medium, and L- for low conductance values). These different conductance values have been attributed to different contact geometries[13] and molecular conformations.[37,38] At low-bias voltages (e.g., 200 mV), the conductance values of H-, M-, and L-junctions agree with the results reported by Li et al.[13] to within 10%, and also with other independent studies,[37,38] as is shown in Table 1.

Summary for Alkanedithiols. We performed similar measurements and analysis for decanedithiol (C10) and hexanedithiol (C6) in order to study the length dependence of the transport properties (Figure S2, SI). The length dependence allowed us to determine the tunneling decay constants, β values (Figure S3, SI).The results are summarized and compared with literature results in Table 1. A small discrepancy is found for the L-junctions conductance of C10 between the present work and that by Li et al.,[13] which is probably due to the relatively low level of current and the broad peak. Except for this discrepancy, the overall agreement between different groups is remarkable, especially considering the history of single-molecule conductance measurements, which indicates good reproducibility of the STM-break junction and statistical analysis for single-molecule conductance measurements.

Biphenyldithiol. In addition to the alkanedithiols, which consist of saturated carbon chains, we studied single-molecule biphenyldithiol junctions.Figure 3a plots an $I-V$ curve histogram of biphenyldithiol created with over 2000 curves, and Figure 3b shows the $G-V$ histogram. Similar to the $G-V$ histograms for alkanedithiols, the $G-V$ histogram of biphenyldithiol shows a clear band. However, an important difference between the two molecular systems is that the $G-V$ band of biphenyldithiol has a much larger curvature near zero bias and looks more like a V-shape, compared to the bowl-shape band found in the alkanedithiols. This difference, as we will discuss later, is due to the increased contribution of frontier

dx.doi.org/10.1021/ja2076857 |J. Am. Chem. Soc. 2011, 133, 19189–19197

Table 1. Comparison of Low-Bias Conductance and Decay Constants between the Present Work and Literature

				literature					
				ref 13		ref 37		ref 38	
molecular junctions		$G(G_0)$	β_N	$G(G_0)$	β_N	$G(G_0)$	β_N	$G(G_0)$	β_N
C6	H	1.6×10^{-3}	1.00 ± 0.20	1.2×10^{-3}	0.96 ± 0.15	1.1×10^{-3}	1.07 ± 0.05	NA	NA
	M	4.5×10^{-4}	1.04 ± 0.17	2.6×10^{-4}	0.94 ± 0.05	2.8×10^{-4}	1.07 ± 0.05	NA	NA
	L	4.8×10^{-5}	0.95 ± 0.19	3.2×10^{-5}	0.45 ± 0.09	NA	NA	NA	NA
C8	H	2.8×10^{-4}	1.00 ± 0.20	2.7×10^{-4}	0.96 ± 0.15	2.5×10^{-4}	1.07 ± 0.05	2.2×10^{-4}	$0.93 \pm 0.05^*$
	M	5.9×10^{-5}	1.04 ± 0.17	5.7×10^{-5}	0.94 ± 0.05	5.2×10^{-5}	1.07 ± 0.05	4.9×10^{-5}	$0.89 \pm 0.03^*$
	L	1.1×10^{-5}	0.95 ± 0.19	1.2×10^{-5}	0.45 ± 0.09	NA	NA	1.2×10^{-5}	$0.89 \pm 0.03^*$
C10	H	2.7×10^{-5}	1.00 ± 0.20	2.2×10^{-5}	0.96 ± 0.15	2.0×10^{-5}	1.07 ± 0.05		$0.93 \pm 0.05^*$
	M	6.9×10^{-6}	1.04 ± 0.17	5.8×10^{-6}	0.94 ± 0.05	4.0×10^{-6}	1.07 ± 0.05		$0.89 \pm 0.03^*$
	L	1.0×10^{-6}	0.95 ± 0.19	2.8×10^{-6}	0.45 ± 0.09	NA	NA		$0.89 \pm 0.03^*$
biphenyl		1.9×10^{-4}	NA	1.8×10^{-4} (ref 42)					

* Extrapolated from a series including longerchains.

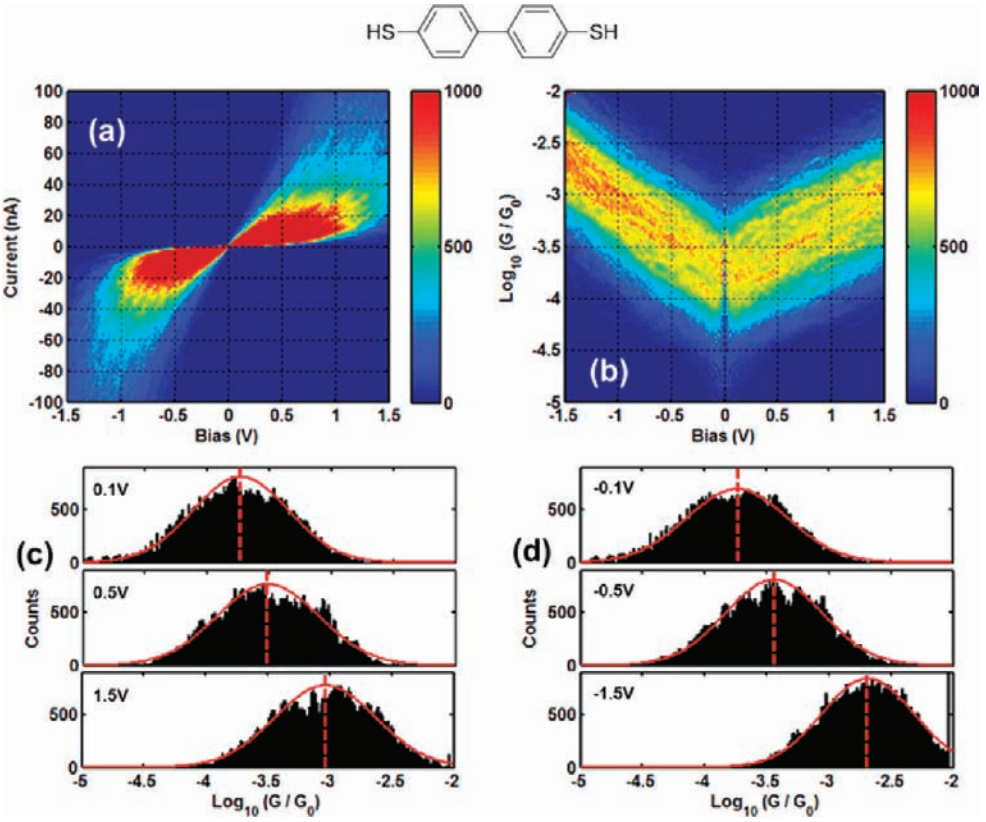

Figure 3. $I-V$ (a) and $G-V$ (b) histograms for biphenyldithiol consisting of 1258 curves. (c) 1-D conductance histogram at different positive (c) and negative (d) bias voltages.

molecular orbitals in biphenyldithiol. One-dimensional conductance histograms at different bias voltages are plotted in Figure 3c. Each histogram shows a pronounced peak, which is in contrast to the multiple peaks in alkanedithiols. The origin for this difference between the two systems is not understood. The peak shifts toward higher conductance values with the bias voltage, indicating strongly nonlinear $I-V$ characteristics for biphenyldithiol. At low biases (e.g., 100 mV), the conductance value is in good agreement with the value reported by Mishchenko et al.[42] However, at higher biases, there is a small but reproducible asymmetry in the $I-V$ curves (Figure 3a). The asymmetry is shown more clearly in the $G-V$ histogram (Figure 3b) and 1-D conductance histograms at positive and negative bias voltages (Figure 3c,d). We will return to this asymmetry later.

Transition Voltage Spectroscopy. So far we have shown that the new STM break junction method allows us to obtain large numbers of $I-V$ and $G-V$ curves, and to perform a statistical analysis on the charge transport characteristics. At low-bias voltages,

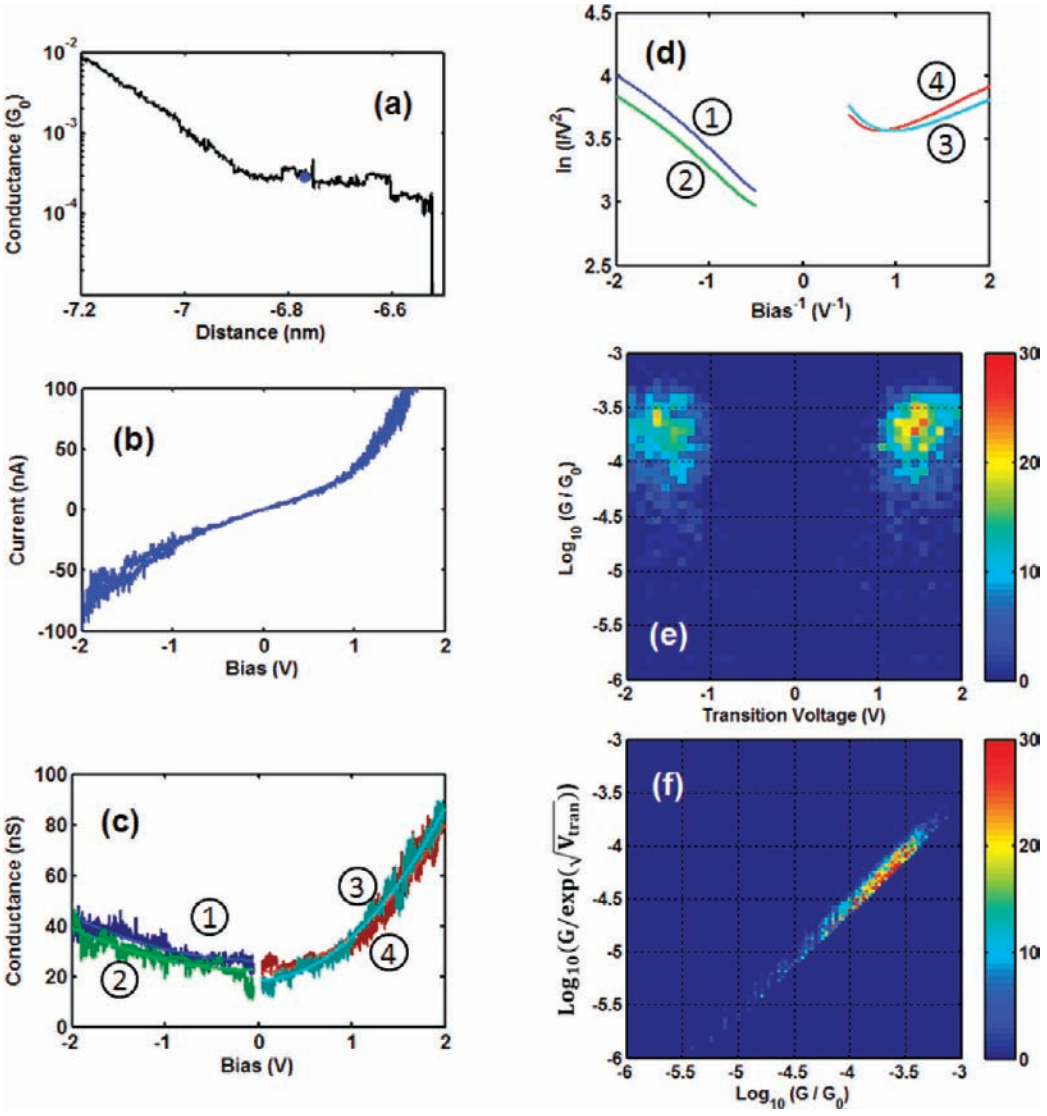

Figure 4. Transition voltage spectroscopy (TVS) and histograms. (a) Typical conductance trace for an H-junction of C8. (b) An $I-V$ curve recorded at the position marked by a blue spot in (a). (c) $G-V$ curves and fittings (smooth curves with lighter colors). (d) Corresponding TVS with colors matching the $G-V$ curves in (c). (e) A 2-D histogram showing the distribution of transition voltage vs low-bias conductance. (f) Correlation between contact conductance vs low-bias conductance.

the $G-V$ histograms recover the results of the previous STM break junction works that measured conductance histogram at a fixed bias, but the $I-V$ characteristic curve and $G-V$ histograms provide much more information. We show below that this method also makes it possible to perform single-molecule transition voltage spectroscopy (TVS), and more importantly, to perform a statistical analysis on thousands of TVS curves. TVS has been introduced recently[24−28] to address one of the most important issues in molecular electronics, tunneling barrier height or the relative alignment of the molecular energy levels with the electrode Fermi energy levels. Energy level alignment determines the charge transport efficiency and mechanism through a molecular junction.

TVS refers to the $\ln(I/V^2)$ vs $1/V$ plot, or the so-called Fowler−Nordheim plot used to study the tunneling to field emission transition in solid-state junctions.[43] Such a transition is indicated by a minimum in the Fowler−Nordheim plot, and the position of the minimum is called the transition voltage, V_{tran}. Beebe et al.[24] have shown that the TVS of thin film molecular junctions also develops a minimum and that the corresponding V_{tran} is proportional to the relative difference between the highest occupied molecular orbital (HOMO) energy level and the Fermi energy ($E_{homo} - E_F$), where E_{homo} and E_F are the HOMO[2,31,44] of the molecule and the Fermi energy of the electrode, respectively. TVS does not depend on a detailed microscopic model and has thus become a convenient and quantitative tool to compare the $I-V$ characteristics of the different molecular systems and to extract important information, such as the energy level alignment.[27,28,31]

To obtain TVS, we started with individual $G-V$ curves (Figure 4). As an example, Figure 4a shows a typical current trace showing a conductance step for an H-junction of C8, and Figure 4b shows two $I-V$ curves (overlaid) recorded at the position marked by a blue spot in Figure 4a. The corresponding $G-V$ curves are presented in Figure 4c, which show high-frequency noise that would be amplified in the TVS plots. Since transition voltage in TVS is determined by nonlinearity of $I-V$ characteristics (low-frequency data), each $G-V$ curve was fit

Table 2. Summary of Transition Voltage, Correlation Coefficients and Asymmetry Ratio of Alkanedithiols and Biphenyldithiol

		transition voltage				
		tip(−)sub(+)		tip(+)sub(−)		asymmetry ratio
molecular junctions		V_{tran} (V)	corr(G, V_{tran})	V_{tran} (V)	corr(G, V_{tran})	$I_{Sub(+)}/I_{Sub(-)}$
C6	H	NA	NA	NA	NA	1.02(@0.5 V)
	M	NA	NA	NA	NA	1.04(@0.5 V)
	L	1.16 ± 0.15	−0.025	1.22 ± 0.16	0.031	1.07(@0.5 V), 1.22(@2 V)
C8	H	1.42 ± 0.32	−0.020	1.49 ± 0.30	0.018	1.22(@2 V)
	M	1.40 ± 0.29	0.23	1.41 ± 0.30	−0.18	1.05(@2 V)
	L	1.10 ± 0.32	0.055	1.12 ± 0.27	−0.18	1.10(@2 V)
C10	H	1.36 ± 0.25	0.0070	1.41 ± 0.28	−0.027	1.07(@2 V)
	M	1.33 ± 0.32	−0.0036	1.40 ± 0.30	0.040	1.04(@2 V)
	L	1.07 ± 0.20	−0.032	1.17 ± 0.18	0.00052	1.12(@2 V)
biphenyl		0.79 ± 0.20	0.0016	0.59 ± 0.08	−0.065	0.45(@1.5 V)

(singular value decomposition) with a smooth second-order polynomial as shown by the solid lines in Figure 4c (the mean squared error normalized by average current is less than 0.2), and from this fitting the TVS curves, or $\ln(G/V)$ vs $1/V$ plots, were determined and are presented in Figure 4d. Minima in the positive bias region are clearly visible (but not in the negative bias region due to the asymmetry of this particular molecular junction). We developed an algorithm to automatically extract the TVS and determine the minimum position, transition voltage, from thousands of $G-V$ curves. This approach allowed us to perform a statistical analysis of transition voltages for molecular junctions with different contact geometries. Figure 4e shows the histogram of the transition voltage distribution vs low-bias conductance (conductance at 200 mV) for the H-conductance value of C8.

Discussion of Transition Voltage Histogram. Several important conclusions can be drawn from such a statistical presentation of the transition voltage. First, the distribution has a maximum count at a transition voltage (Figure 4e), which will be referred to as the most probable, or peak transition, voltage. For the H-conductance of C8, the peak transition voltage is 1.4 V, which is consistent with the value found for thin film alkane monothiols.[25] The value is smaller than the transition voltage for a vacuum tunneling junction,[29] indicating a lower tunneling barrier via the molecule than that via vacuum. Second, there is a distribution with a half width at half-maximum (HWHM) of ∼0.25 V in the transition voltage obtained from thousands of molecular junctions with different molecule−electrode contact geometries. This fact indicates that the alignment of the molecular energy level relative to the electrode Fermi level varies from junction to junction, and depends on the contact geometry. In other words, the molecule−electrode contact geometry affects the conductance of a molecular junction not only because of the contact resistance change (electronic coupling efficiency) but also through the energy level alignment (barrier height). Note that the bias voltage profile across the molecular junction may also vary from junction to junction, thus affecting the distribution of the transition voltage.[45] However, most of the voltage drop is expected to take place at the molecule−electrode contacts as indicated by the lack of molecular length dependence of the transition voltage found here and in ref 25. Also associated with the bias voltage drop at each of the two contacts is an electric dipole, which affects the barrier height, and is already taken into account in the analysis.

Even though there is a significant junction-to-junction variation in the transition voltage, the low-bias conductance value within a given conductance peak (H-, M-, or L-) is not strongly correlated with the transition voltage. For example, in the case of C8 shown in Figure 4e, we found a correlation coefficient of 0.02, which means there is almost no correlation between low-bias conductance and the energy level alignment. Similarly, the correlation coefficients for other molecular junctions are also small (Table 2).This conclusion may seem counterintuitive at first glance. If we assume a model where the molecule acts as a tunneling barrier, then the conductance can be defined as $G = A(e^{-\beta L})$, where A is the contact conductance, β is the tunneling decay constant, L is the length, and β^2 is proportional to V_{tran}.[24,46] As such, one would expect that any changes in V_{tran} would correlate strongly with the conductance. The absence of correlation between G and V_{tran} in the experimental data means that the large conductance variation is primarily due to variation in A, the contact resistance, rather than due to β or V_{tran}. In fact, the HWHM of V_{tran} distribution is rather narrow; e.g., it is ∼0.25 V or ∼18% for C8 H- and M-junctions. Since $\beta \approx V_{tran}^{1/2}$ according to the above model, the corresponding variation in β is ∼10%, which could contribute only ∼10% to the conductance variation. The actual observed low-bias conductance variation is at least an order of magnitude greater than 10%, so most of it must be due to the contact resistance variation, rather than variation in V_{tran}.

To further confirm above conclusion, we have also calculated the correlation coefficient between the conductance and the contact conductance by plotting the $\log(G/e^{V_{tran}})$, which is $(\sim\log(A))$ vs $\log(G)$, as is shown in Figure 4f, and found a value of 0.98 (see SI for more details), thus indicating that the low-bias conductance is strongly correlated with the contact resistance. This indicates that the distribution of contact resistance varies over a much larger range than the tunneling barrier height, and as such any correlation with the transition voltage is obfuscated by the large distribution of contact resistance. This result illustrates the capability of the current approach to determine contributions from both the contact resistance and the energy level alignment, which is in contrast to the previous single-bias measurement that cannot separate the two contributions.

Figure 5 summarizes the statistical analysis of the transition voltages for H-, M-, and L-molecular junctions of C8 and C10. For C6, only the transition voltages for L-junctions could be measured due to the instability of H- and M- junctions of C6 at high

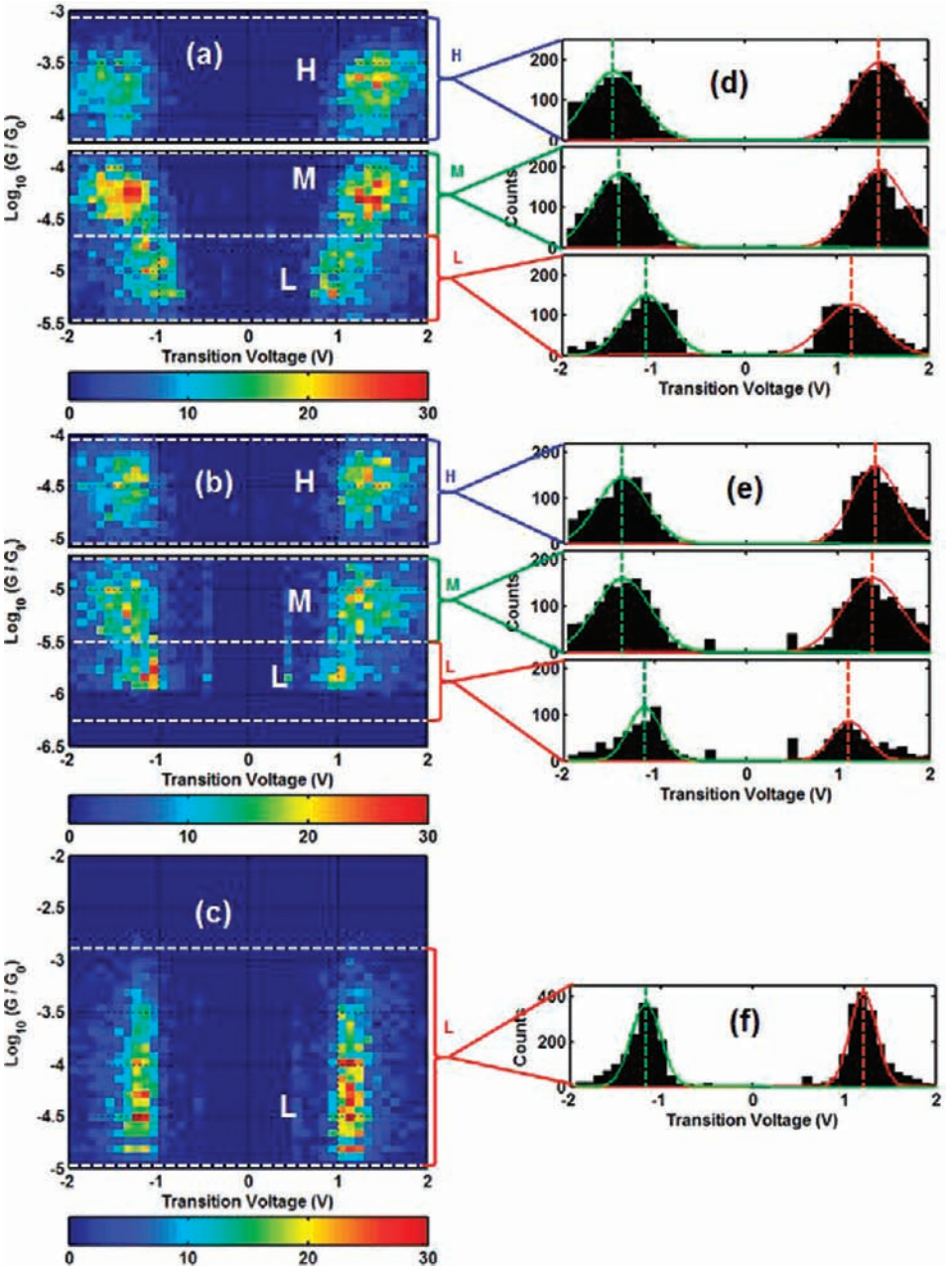

Figure 5. Transition voltage histograms for C8, C10, and C6. (a−c) 2-D transition voltage histograms for C8 H, M, and L, C10 H, M, and L and C6 L junctions. (d−f) 1-D histograms summing up the counts between white dash lines in (a−c).

bias voltages. The transition voltages for H- and M-junctions are similar (∼1.4) despite their large conductance difference, which indicates that H- and M-junctions are due to difference in contact resistance rather than energy level alignment. This observation is consistent with the above conclusion that the contact resistance is the primary cause of the large conductance variation in single molecules. In contrast to H- and M-junctions, the transition voltage forL-junctions is ∼1.1 V, which is significantly smaller. The smaller transition voltage is also reflected by the larger curvature in the $G-V$ curves for the L-junctions, compared to the H- and M-junctions as shown in Figure 3. It is also consistent with the smaller β value for the L-junctions. If assuming tunneling through a barrier model, then β should be proportional to the square root of the barrier height and one should compare β^2 with the transition voltages. The ratio for β^2 between the M- and L-junctions is ∼1.2, which agrees with the corresponding ratio for the transition voltages (∼1.27). We caution that given the error bars in the β values, this analysis mainly serves the purpose of consistency check between the transition voltages and β values.

Summary for alkanedithiols. Similar results were also obtained for C10, which are summarized together with the data for C6 and C8 in Table 2. The difference in the transition voltage values for C6 (L-junctions), C8 and C10 are small, indicating that they are insensitive to the molecular length, which agrees with the finding by Beebe et al.[25] for self-assembled alkanemonothiol layers, as we mentioned earlier. The transition voltages for C6, C8 and C10 for L-junctions show consistently smaller values than those for H- and M-junctions, which indicatesthe difference between the

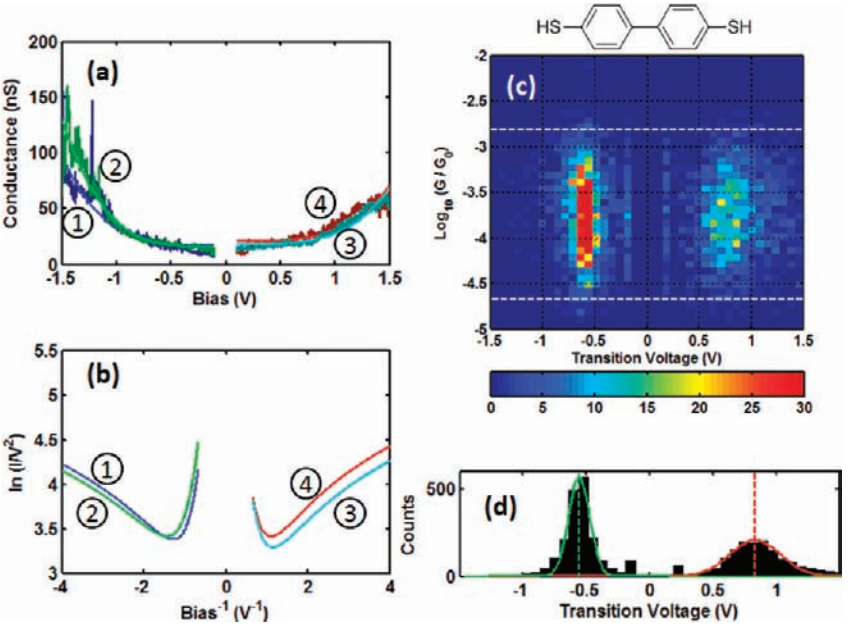

Figure 6. TVS of biphenyldithiol. (a) $G-V$ curves and fittings. (b) TVS curves determined from the $G-V$ curves in (a). (c) 2-D transition voltage histogram. (d) 1-D histograms summing up the counts between white dash lines in (a–c).

HOMO and the electrode Fermi energy[31] for L-junctions are smaller than those of H- and M-junctions, despite their lower conductance values. Although this observation seems to be surprising because one would expect a lower conductance to yield a higher V_{tran}, it is consistent with previous first-principles calculations.[13] The L-junctions have been attributed to a gauche conformation by Li et al.,[13] and the *ab initio* calculation showed a smaller HOMO-Fermi gap for the L-junctions. This result further indicates that HOMO-Fermi energy alignment is not the only parameter that determines the conductance of a molecular junction.

Biphenyldithiol. To further demonstrate the value of single-molecule TVS, we measured the TVS of biphenyldithiol. The molecule consists of two aromatic rings linked together with a torsion angle of 36.5°.[21] Previous studies of phenyl systems with different numbers of phenyl rings indicate a smaller tunneling decay constant than in alkane chains.[21] Figure 6 shows the transition voltage distribution of over 2000 biphenyldithiol junctions vs voltage and conductance. The most probable transition voltage is about 0.7 V, which is significantly smaller than the value for the alkanedithiols. The smaller transition voltage is expected if one considers the lower-energy π-electrons of the aromatic rings in biphenyldithiol in contrast to the σ-electrons dominating the alkanedithiols. The smaller V_{tran} is also consistent with the observation of smaller tunneling decay constants in phenyl systems.[21]

Discussion on Asymmetry. All of the molecules studied here are symmetric, but many of the individual $I-V$ and $G-V$ curves display asymmetry, as we noted earlier. The asymmetry is also clearly seen in the transition voltage histograms (e.g., Figure 6c). To examine the statistical significance of the asymmetry, we determined the distribution of the asymmetry factor vs the conductance, where the asymmetry factor is defined as the ratio of current at a large forward bias to that at a large reverse bias. For alkanedithiols, the most probable asymmetry factors are close to 1. However, for biphenyldithiol the asymmetry factor is 0.45, indicating a large asymmetry. We have analyzed this asymmetry quantitatively and presented the findings in Table 2 and in the SI (Figure S3). For a given molecule, the asymmetry always has the same polarity, which leads us to believe that it originated from the asymmetry of the electrodes, namely the relatively flat substrate electrode vs the sharp tip electrode. The relatively large asymmetry in biphenyldithiol may be attributed to the stronger coupling of the π-electrons of the aromatic rings to the flat substrate than to the atomically sharp tip, as we have recently reported in other molecular systems.[47] Further studies are clearly needed in order to fully understand the nature of the observed asymmetry, but the ability to measure and perform a statistical analysis on a large number of molecular junctions with different contact geometries over a wide bias range makes the asymmetry studies possible and statistical analysis meaningful.

SUMMARY AND CONCLUSIONS

In conclusion, a new STM break junction method was developed for the rapid measurement of thousands of $I-V$ and $G-V$ curves of repeatedly created single-molecule junctions, thus allowing the construction and analysis of $I-V$ and $G-V$ histograms. The low-bias conductance values reproduced those obtained by measuring the conductance at small fixed biases as reported in literature. However, the present method provides complete $I-V$ and $G-V$ curves, revealing nonlinear regimes and asymmetry, and allowing for statistical analyses of the results. More importantly, transition voltage spectroscopy of single-molecule junctions was carried out to determine transition voltage, an important parameter that quantifies the alignment of molecular energy levels relative to electrode Fermi levels. The transition voltages of alkanedithiols peak at 1.4 V for the H- and M-junctions, and 1.1 V for the L-junctions, and these values are independent of the molecular length (n = 6, 8, and 10). For biphenyldithiol, the transition voltage is 0.7 V, much lower than for the alkanedithiols. There is a significant distribution in the transition voltage for the repeatedly created individual molecular junctions, which indicates the dependence of the molecular energy level alignment on the molecule–electrode contact geometry.

However, the variation in single-molecule conductance values is mainly due to contact resistance rather than energy level alignment variations. This work adds a new dimension (voltage) to the widely used conductance histogram analysis approach for single-molecule transport studies, and allows for a better understanding of the charge transport characteristics. This method is anticipated to significantly benefit the study of single-molecule charge transport in other molecular systems.

■ ASSOCIATED CONTENT

Supporting Information. Additional figures and experimental details. This material is available free of charge via the Internet at http://pubs.acs.org.

■ AUTHOR INFORMATION

Corresponding Author
njtao@asu.edu

■ ACKNOWLEDGMENT

Financial support for this work has been provided by the NSF (ECCS0925498, and CHE1105558). I.D.-P. thanks the Ramony Cajal program from the MICINN for financial support.

■ REFERENCES

(1) Song, H.; Reed, M. A.; Lee, T. *Adv. Mater.* **2001**, *23*, 1583.
(2) Nitzan, A.; Ratner, M. A. *Science* **2003**, *300*, 1384.
(3) Tao, N. J. *Nat. Nanotechnol.* **2006**, *1*, 173.
(4) McCreery, R. L. *Chem. Mater.* **2004**, *16*, 4477.
(5) Smit, R. H. M.; Noat, Y.; Untiedt, C.; Lang, N. D.; van Hemert, M. C.; van Ruitenbeek, J. M. *Nature* **2002**, *419*, 906.
(6) Gonzalez, M. T.; Wu, S. M.; Huber, R.; van der Molen, S. J.; Schonenberger, C.; Calame, M. *Nano Lett.* **2006**, *6*, 2238.
(7) Loertscher, E.; Weber, H. B.; Riel, H. *Phys. Rev. Lett.* **2007**, *98*, 176807.
(8) Xu, B. Q.; Tao, N. J. *Science* **2003**, *301*, 1221.
(9) Haiss, W.; Van Zalinge, H.; Higgins, S. J.; Bethell, D.; Hoebenreich, H.; Schiffrin, D. J.; Nichols, R. J. *J. Am. Chem. Soc.* **2003**, *125*, 15294.
(10) Jang, S. Y.; Reddy, P.; Majumdar, A.; Segalman, R. A. *Nano Lett.* **2006**, 2362.
(11) Lindsay, S. M.; Ratner, M. A. *Adv. Mater.* **2007**, *19*, 23.
(12) Hylke, B. A.; Bert de, B. *J. Phys.: Condens. Matter* **2008**, *20*, 013001.
(13) Li, C.; Pobelov, I.; Wandlowski, T.; Bagrets, A.; Arnold, A.; Evers, F. *J. Am. Chem. Soc.* **2008**, *130*, 318.
(14) Paulsson, M.; Krag, C.; Frederiksen, T.; Brandbyge, M. *Nano Lett.* **2008**, *9*, 117.
(15) Muller, K. H. *Phys. Rev. B* **2006**, *73*, 045403.
(16) Huang, Z. F.; Chen, F.; Bennett, P. A.; Tao, N. J. *J. Am. Chem. Soc.* **2007**, *129*, 13225.
(17) Arroyo, C. R.; Leary, E.; Castellanos-Gomez, A.; Rubio-Bollinger, G.; Gonzalez, M. T.; Agrait, N. *J. Am. Chem. Soc.* **2011**, *133*, 14313.
(18) Frei, M.; Aradhya, S. V.; Koentopp, M.; Hybertsen, M. S.; Venkataraman, L. *Nano Lett.* **2011**, *11*, 1518.
(19) Kamenetska, M.; Koentopp, M.; Whalley, A. C.; Park, Y. S.; Steigerwald, M. L.; Nuckolls, C.; Hybertsen, M. S.; Venkataraman, L. *Phys. Rev. Lett.* **2009**, *102*, 126803.
(20) Park, Y. S.; Whalley, A. C.; Kamenetska, M.; Steigerwald, M. L.; Hybertsen, M. S.; Nuckolls, C.; Venkataraman, L. *J. Am. Chem. Soc.* **2007**, *129*, 15768.
(21) Venkataraman, L.; Klare, J. E.; Nuckolls, C.; Hybertsen, M. S.; Steigerwald, M. L. *Nature* **2006**, *442*, 904.
(22) Tsutsui, M.; Shoji, K.; Taniguchi, M.; Kawai, T. *Nano Lett.* **2007**, *8*, 345.
(23) Tsutsui, M.; Taniguchi, M.; Kawai, T. *J. Am. Chem. Soc.* **2009**, *131*, 10552.
(24) Beebe, J. M.; Kim, B.; Gadzuk, J. W.; Frisbie, C. D.; Kushmerick, J. G. *Phys. Rev. Lett.* **2006**, *97*, 026801.
(25) Beebe, J. M.; Kim, B.; Frisbie, C. D.; Kushmerick, J. G. *ACS Nano* **2008**, *2*, 827.
(26) Bennett, N.; Xu, G. Z.; Esdaile, L. J.; Anderson, H. L.; Macdonald, J. E.; Elliott, M. *Small* **2010**, *6*, 2604.
(27) Huisman, E. H.; Guedon, C. M.; van Wees, B. J.; van der Molen, S. J. *Nano Lett.* **2009**, *9*, 3909.
(28) Markussen, T.; J.Z., C.; Thygesen, K. S. *Phys. Rev. B* **2011**, *83*, 155407.
(29) Trouwborst, M. L.; Martin, C. A.; Smit, R. H. M.; Guedon, C. M.; Baart, T. A.; van der Molen, S. J.; van Ruitenbeek, J. M. *Nano Lett.* **2011**, *11*, 614.
(30) Pakoulev, A. V.; Burtman, V. *J. Phys. Chem. C* **2009**, *113*, 21413.
(31) Song, H.; Kim, Y.; Jang, Y. H.; Jeong, H.; Reed, M. A.; Lee, T. *Nature* **2009**, *462*, 1039.
(32) Xu, B. Q.; Xiao, X. Y.; Tao, N. J. *J. Am. Chem. Soc.* **2003**, *125*, 16164.
(33) Teramae, Y.; Horiguchi, K.; Hashimoto, S.; Tsutsui, M.; Kurokawa, S.; Sakai, A. *Appl. Phys. Lett.* **2008**, *93*, 083121.
(34) Díez-Pérez, I.; Hihath, J.; Lee, Y.; Yu, L. P.; Adamska, L.; Kozhushner, A.; Oleynik, I. I.; Tao, N. J. *Nature Chem.* **2009**, *1*, 635.
(35) Huang, Z. F.; Chen, F.; D'Agosta, R.; Bennett, P. A.; Di Ventra, M.; Tao, N. J. *Nat. Nanotechnol.* **2007**, *2*, 698.
(36) Di Ventra, M.; Pantelides, S. T.; Lang, N. D. *Phys. Rev. Lett.* **2002**, *88*, 046801/1.
(37) Li, X.; He, J.; Hihath, J.; Xu, B.; Lindsay, S. M.; Tao, N. *J. Am. Chem. Soc.* **2006**, *128*, 2135.
(38) Haiss, W.; Martin, S.; Leary, E.; van Zalinge, H.; Higgins, S. J.; Bouffier, L.; Nichols, R. J. *J. Phys. Chem. C* **2009**, *113*, 5823.
(39) González, M. T.; Brunner, J.; Huber, R.; Wu, S.; Schönenberger, C.; Calame, M. *New J. Phys.* **2008**, *10*, 065018.
(40) Joshua, H.; Nongjian, T. *Nanotechnology* **2008**, *19*, 265204.
(41) Hihath, J.; Bruot, C.; Tao, N. *ACS Nano* **2010**, *4*, 3823.
(42) Mishchenko, A.; Vonlanthen, D.; Meded, V.; Burkle, M.; Li, C.; Pobelov, I.; Bagrets, A.; Viljas, J.; Pauly, F.; Evers, F.; Mayor, M.; Wandlowski, T. *Nano Lett.* **2010**, *10*, 156.
(43) Fowler, R. H.; Nordheim, L. *Proc. R. Soc. London. Ser. A* **1928**, *119*, 173.
(44) Lawson, J. W.; Bauschlicher, C. W. *Phys. Rev. B* **2006**, *74*, 125401.
(45) Mirjani, F.; Thijssen, J. M.; van der Molen, S. J. *Phys. Rev. B* **2011**, *84*, 115402.
(46) Simmons, J. G. *J. Appl. Phys.* **1963**, *34*, 2581.
(47) Díez-Pérez, I.; Hihath, J.; Hines, T.; Wang, Z. S.; Zhou, G.; Müllen, K.; Tao, N. J. *Nat. Nanotechnol.* **2011**, *6*, 226.